Relationship between topological order and glass forming ability in densely packed enstatite and forsterite composition glasses

S. Kohara[a], J. Akola[b,c,d], H. Morita[e], K. Suzuya[f], J. K. R. Weber[g,h], M. C. Wilding[i], and C. J. Benmore[h,1]

[a]Research and Utilization Division, Japan Synchrotron Radiation Research Institute/SPring-8, 1-1-1 Kouto, Sayo-cho, Sayo-gun, Hyogo 679-5198, Japan; [b]Department of Physics, Tampere University of Technology, P.O. Box 692, FI-33101, Tampere, Finland; [c]Department of Physics, Nanoscience Center, University of Jyväskylä, P.O. Box 35, FI-40014, Jyväskylä, Finland; [d]Institut für Festkörperforschung, Forschungszentrum Jülich, D-52425 Jülich, Germany; [e]Graduate School of Science and Engineering, Yamagata University, 1-4-12 Kojirakawa, Yamagata-City, Yamagata 990-8560, Japan; [f]Japan Proton Accelerator Research Complex Center, Japan Atomic Energy Agency, Tokai-mura, Naka-gun, Ibaraki 319-1195, Japan; [g]Materials Development, 3090, Daniels Court, Arlington Heights, IL 60004; [h]Advanced Photon Source, Argonne National Laboratory, Argonne, IL 60439; and [i]Center for Advanced Functional Materials and Devices, Institute of Mathematics and Physics, Aberystwyth University, Aberystwyth SY23 3BZ, United Kingdom

Edited by Frans Spaepen, Harvard, Cambridge, MA, and accepted by the Editorial Board July 19, 2011 (received for review March 25, 2011)

The atomic structures of magnesium silicate melts are key to understanding processes related to the evolution of the Earth's mantle and represent precursors to the formation of most igneous rocks. Magnesium silicate compositions also represent a major component of many glass ceramics, and depending on their composition can span the entire fragility range of glass formation. The silica rich enstatite ($MgSiO_3$) composition is a good glass former, whereas the forsterite (Mg_2SiO_4) composition is at the limit of glass formation. Here, the structure of $MgSiO_3$ and Mg_2SiO_4 composition glasses obtained from levitated liquids have been modeled using Reverse Monte Carlo fits to diffraction data and by density functional theory. A ring statistics analysis suggests that the lower glass forming ability of the Mg_2SiO_4 glass is associated with a topologically ordered and very narrow ring distribution. The MgO_x polyhedra have a variety of irregular shapes in $MgSiO_3$ and Mg_2SiO_4 glasses and a cavity analysis demonstrates that both glasses have almost no free volume due to a large contribution from edge sharing of MgO_x-MgO_x polyhedra. It is found that while the atomic volume of Mg cations in the glasses increases compared to that of the crystalline phases, the number of Mg-O contacts is reduced, although the effective chemical interaction of Mg^{2+} remains similar. This unusual structure-property relation of Mg_2SiO_4 glass demonstrates that by using containerless processing it may be possible to synthesize new families of dense glasses and glass ceramics with zero porosity.

Earth science | glass structure

Glasses can be synthesized by making use of a network former, such as B_2O_3, As_2O_3, SiO_2, GeO_2, or P_2O_5 which form continuous three-dimensional networks, according to Zachariasen's theory (1). On the basis of this theory many ideas on glass formation have been proposed. One such idea by Cooper and Gupta proposed that a topologically disordered network is the key to understanding the origin of glass formation (2, 3). Indeed, it is well known that the silica glass network exhibits a broad ring distribution which is topologically disordered, and is made up of a connection of SiO_4 tetrahedra sharing oxygen atoms at the corners (4, 5). In contrast the corresponding crystalline phase has only 6-fold rings.

Recently the use of the aerodynamic levitation technique combined with a laser heating system has expanded the glass forming range of many oxides, due to the avoidance of contact between the container walls and high-temperature melt (6). Tangeman and coworkers succeeded in synthesizing MgO-SiO_2 glasses over a wide compositional range (7), covering the enstatite composition ($MgSiO_3$) to the forsterite composition (Mg_2SiO_4), which can be considered as analogues of quenched melts from the Earth and Lunar mantle (8–10). The Mg_2SiO_4 composition glass has been formerly synthesized using a rapid quench method and studied using vibrational spectroscopy (11, 12), however, the advantage of the levitation technique is that it allows us to synthesize a high-purity bulk sample. The structure of these glasses was recently studied using theoretical simulation (13), spectroscopic measurements (7, 13–15), diffraction measurements (16–19), and atomistic modeling on the basis of diffraction data (17–19). Using Reverse Monte Carlo (RMC) modeling (20) Kohara, et al. discovered that SiO_4 tetrahedra formed both monomers (isolated SiO_4) and dimers (Si_2O_7) in Mg_2SiO_4 glass, and that the network structure of the glass largely comprises of MgO_x polyhedra with both corner and edge-sharing oxygens (17). Sen and Tangeman confirmed from the results of molecular dynamics simulation that the presence of a large excess of bridging O atoms associated with the Si_2O_7 dimers in Mg_2SiO_4 glass and melt, is in sharp contrast with their complete absence in the crystalline phase (13). By combining neutron and X-ray diffraction data Wilding et al. reported a relatively small but abrupt change in the average Mg-O coordination number from 4.5 to 5.0 over the narrow composition range 38 mol% SiO_2 to 33 mol% SiO_2 (Mg_2SiO_4); both coordination numbers being significantly smaller than the octahedral Mg coordination which occurs in the corresponding crystalline phases (16). This result is in agreement with the RMC Mg_2SiO_4 model by Kohara et al. which yielded an average Mg-O coordination number of 4.95. However, the diffraction and RMC results are in disagreement with recent NMR measurements that suggest MgO_6 octahedra are dominant in both $MgSiO_3$ and Mg_2SiO_4 glasses (14, 15), leading to two vastly different structural models.

In this paper we model and analyze the structure of silica glass (SiO_2), enstatite glass ($MgSiO_3$), and forsterite (Mg_2SiO_4) glass employing the RMC modeling technique and the density function theory (DFT) of electronic structure using measured and published synchrotron X-ray and neutron diffraction data (16–18). Special attention is paid to ring statistics, cavity volumes, and the connectivity of short-range structural units in the glasses. We also analyze the chemical nature of the Mg-O interaction in these systems to explain the different atomistic models arrived at on the basis of diffraction and NMR data to reveal the relationship between "topological order-disorder" and "glass forming ability."

Author contributions: S.K. designed research; S.K., J.A., H.M., K.S., J.K.R.W., and M.W.C. performed research; S.K., H.M., and J.A. analyzed data; and S.K., J.A., and C.J.B. wrote the paper.

The authors declare no conflict of interest.

This article is a PNAS Direct Submission. F.S. is a guest editor invited by the Editorial Board.

[1]To whom correspondence should be addressed. E-mail: benmore@aps.anl.gov.

This article contains supporting information online at www.pnas.org/lookup/suppl/doi:10.1073/pnas.1104692108/-/DCSupplemental.

RMC Modeling

RMC modeling was performed using the RMCA code (20). Because the structural model for SiO_2 glass and Mg_2SiO_4 glass have been reported previously (5, 17), an RMC simulation was performed on an ensemble of 4,800 particles for $MgSiO_3$ glass. The starting configuration was created using hard sphere Monte Carlo (HSMC) simulations with constraints applied to avoid a physically unrealistic structure. Two kinds of constraints were used: closest atom-atom approach and connectivity. The choices of the closest atom-atom approaches were determined to avoid unreasonable spikes in the partial-pair correlation functions. The constraint on the Si-O connectivity was that all silicon atoms were coordinated to four oxygen atoms, but no constraint on the Mg-O connectivity was applied. After the HSMC simulations, RMC simulations with both X-ray and neutron $S(Q)$ were performed. The atomic number density used was 0.08218 $Å^{-3}$ (16).

DFT Simulations. The geometry optimizations and electronic structure calculations of $MgSiO_3$ and Mg_2SiO_4 glasses are performed using the CP2K program (21, 22) in DFT mode. The starting configurations of the 510 ($MgSiO_3$) and 511-atom (Mg_2SiO_4) models of glass phases have been generated by RMC modeling using the experimental densities (Fig. S1). Central in the CP2K method is the use of two representations of the electron density: localized Gaussian and plane wave (GPW) basis sets. This representation allows for an efficient treatment of the electrostatic interactions, and leads to a scheme that is formally linearly scaling as a function of the system size. The valence electron—ion interaction is based on the norm-conserving and separable pseudopotentials of the analytical form derived by Goedecker, Teter, and Hutter (23). We considered the following valence configurations: O ($2s^22p^4$), Mg ($2s^22p^63s^2$), and Si ($3s^23p^2$). For the Gaussian based (localized) expansion of the Kohn-Sham orbitals we use a library of contracted m-DZVP basis sets (24), and the complementary plane wave basis set has a cut-off of 600 Ry [1 Rydberg (Ry) equals to 13.6 eV] for electron density (this equals to 150 Ry for wave functions in standard plane wave schemes). The molecularly optimized m-DZVP functions result in highly accurate results with less computational cost as experienced with the traditional basis sets that are fitted to atomic properties. Together with the GPW basis set this enables DFT simulations of systems up to 1,000 atoms or more. The increased performance is crucial for amorphous (glassy) materials as it is desirable to reduce the effects of the finite simulation cell (periodic boundary conditions) by increasing the system size and improving the statistics by including more atoms.

The generalized gradient-corrected approximation of Perdew, Burke, and Ernzerhof is adopted for the exchange-correlation energy functional (25). The average cohesive energies of the DFT-optimized crystalline structures of $MgSiO_3$ (320 atoms) and Mg_2SiO_4 (336 atoms) are 5.19 and 5.08 eV/atom, respectively, and the crystalline phase is 0.30 and 0.36 eV/atom more stable than glass. The optimized crystalline geometries are very close to the experimental structures of $MgSiO_3$ (26) and Mg_2SiO_4 (27), and the average Mg-O distances are within 0.01 Å from the experiment (maximum individual deviation 0.05 Å) (Fig. S2). Effective charges of individual atoms have been evaluated from electron density (28) and chemical bond orders between atomic pairs have been computed from the overlaps of the atomic orbital components (with a projected completeness 97.5%).

Ring Statistics and Q_n Calculations. The ring statistics were calculated using the shortest-path analysis (29, 30) and included up to 12-fold rings. The number of atoms were counted that existed in a loop from an atom at a defined starting point, by returning to the same atom through the shortest-path length. This analysis was performed in order to avoid the counting of a large-number of n-fold rings that could be divided into smaller-number m-fold rings, where $m < n$. Furthermore, multiple counting was avoided by checking the linkage in individual rings. In this study we define an n-fold ring as a ring consisting of n polyhedra and define the maximum coordination distance for Si-O correlation to be 1.8 Å for both glasses and the maximum Mg-O correlation distance to be 2.5 Å ($MgSiO_3$ glass) and 2.8 Å (Mg_2SiO_4 glass). It is confirmed that the normalized fraction of ring statistics are insensitive to the distances chosen. To analyze the structural and chemical order within the network in glasses, we characterized the concentration of various types of Si environments. Silicon oxide environments are typically denoted as Q_n species, where n varies between 0 and 4 and denotes the number of bridging oxygens, using atomic configurations obtained by RMC modeling.

Cavity Analysis. The cavity analysis has been performed as described in ref. 31. The system is divided into a cubic mesh with a grid spacing of 0.20 Å, and the points farther from any atom at a given cutoff (here 2.5 Å) are selected and defined as "cavity domains." Each domain is characterized by the point where the distance to all atoms is a maximum. If there are no maxima closer than the di-vacancy cutoff (here 2.0 Å), we locate the center of the largest sphere that can be placed inside the cavity. This point can be used for calculating partial-pair distribution functions, including vacancy-vacancy correlations. Around the cavity domains we construct cells analogous to the Voronoi polyhedra in amorphous phases (cf. the Wigner-Seitz cell) and analyze their volume distribution.

Results and Discussion

The partial structure factors, $S_{SiSi}(Q)$, $S_{SiO}(Q)$, and $S_{OO}(Q)$ of SiO_2, $MgSiO_3$, and Mg_2SiO_4 glasses obtained from the RMC model are shown in Fig. 1. It is well known that SiO_2 glass exhibits the first sharp diffraction peak (FSDP) at approximately $Q = 1.52$ $Å^{-1}$. It is of note that the strong positive contribution of the $S_{OO}(Q)$ in SiO_2 glass to the FSDP becomes smaller and the peak position shifts to higher Q in both $MgSiO_3$ and Mg_2SiO_4 glasses. The $S_{SiO}(Q)$ shows a similar behavior, but the contribution of $S_{SiSi}(Q)$ to the FSDP in Mg_2SiO_4 glass is larger than those in both SiO_2 and $MgSiO_3$ glasses, although the fraction of silicon in Mg_2SiO_4 glass is the smallest. This unusual behavior cannot be observed in total X-ray and neutron data, because the weighting factor of the Si-Si correlation is very small in both cases. However, this behavior suggests significant modification of the

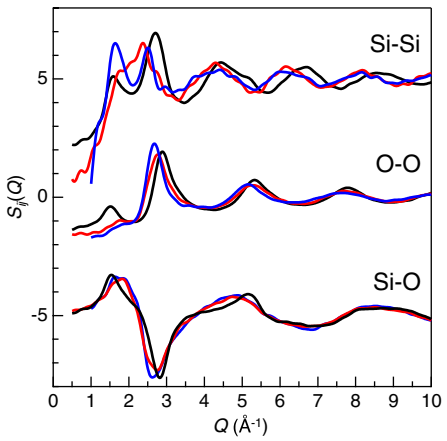

Fig. 1. Partial structure factors, $S_{ij}(Q)$, for $S_{SiSi}(Q)$, $S_{SiO}(Q)$, and $S_{OO}(Q)$ of SiO_2, $MgSiO_3$, and Mg_2SiO_4 glasses obtained from the RMC model. Black line, SiO_2 glass; Red line, $MgSiO_3$ glass; Blue line, Mg_2SiO_4 glass. The experimental X-ray and neutron total structure factors, $S(Q)$, of $MgSiO_3$ and Mg_2SiO_4 glasses together with total $S(Q)$ and partial structure factors, $S_{ij}(Q)$, obtained from RMC modeling are shown in Fig. S3. Partial-pair distribution functions, $g_{ij}(r)$, of $MgSiO_3$ and Mg_2SiO_4 glasses obtained from the RMC model are shown in Fig. S4.

silicate network occurs in Mg_2SiO_4 glass in comparison with SiO_2 glass and $MgSiO_3$, and also in the formation of chemical ordering recently argued by Salmon et al (32). Indeed, according to the RMC simulation reported by Kohara, et al. (17), the SiO_4 network has disappeared in Mg_2SiO_4 glass, which is manifested by significant peak in the $S_{SiSi}(Q)$ as a signature of chemical ordering of silicon. Also, the arrangement of SiO_4 tetrahedra has fewer steric constraints in Mg_2SiO_4 glass due to the deformation of the network. Similar behavior can be seen in 64 mol% PbO-34 mol% SiO_2 glass (33), which can be synthesized by a conventional melt-quench technique.

Fig. 2 shows the distribution of SiO_4 tetrahedra and ring statistics of SiO_4 tetrahedra in SiO_2, $MgSiO_3$, and Mg_2SiO_4 glasses with a typical linkage of 4-fold and 6-fold Si-O rings. As can be seen in Fig. 2*A*, SiO_2 glass forms an SiO_4 network of corner-shared oxygens, providing a very broad ring size distribution and $MgSiO_3$ glass has large fraction of 3-fold and 4-fold rings, showing how the SiO_4 network is modified by the addition of Mg-O. In contrast, Mg_2SiO_4 glass does not form a SiO_4 network and the SiO_4 monomer and Si_2O_7 dimer are the predominant silicate species (17). These behaviors are reflected in the Q_n distribution for SiO_4 tetrahedra. The contribution of Q_1, Q_2, and Q_3 species are all significant in $MgSiO_3$ glass, while that of Q_1 is the most abundant in Mg_2SiO_4 glass. The connectivity analysis (33) also shows that about 14% oxygen in Mg_2SiO_4 glass can be assigned as "free oxygen" that does not participate in silicate fragments (13), which is in sharp contrast to $MgSiO_3$ where the contribution of "free oxygen" is small (~2%). In terms of stoichiometry, the emergence of free oxygen in Mg_2SiO_4 glass is coupled to the existence of bridging oxygens in silicate fragment chains (Q_1, Q_2, and Q_3).

The distribution of MgO_x polyhedra in $MgSiO_3$ and Mg_2SiO_4 glasses and ring statistics are shown in Fig. 3. The Mg-O peak position observed in the $g_{MgO}(r)$ of the RMC model at approximately 2.0 Å in both $MgSiO_3$ and Mg_2SiO_4 glasses (Fig. S4), is shorter than average Mg-O bond length of approximately 2.08 Å ($MgSiO_3$) and 2.13 Å (Mg_2SiO_4) in MgO_6 octahedra found in the corresponding crystal phases (17, 26, 27). This difference suggests that the Mg-O coordination number is ~5 in these glasses on the basis of effective ionic radii (34). In the case of $MgSiO_3$ glass, the RMC model suggests that MgO_4 is the major unit, which is

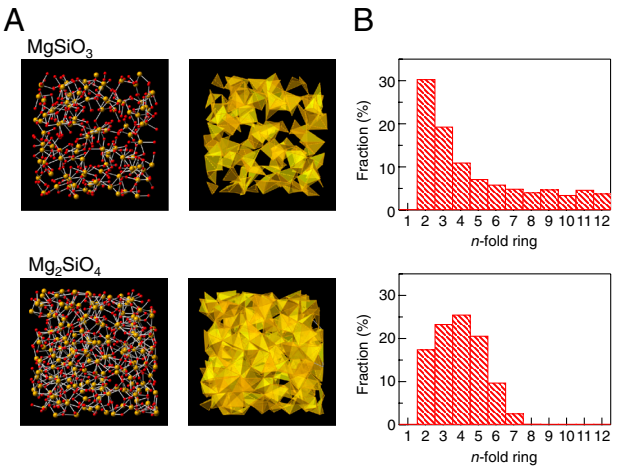

Fig. 3. The distribution of MgO_x polyhedra (*A*) and ring statistics (*B*) in $MgSiO_3$ and Mg_2SiO_4 glasses (maximum correlation distance is 2.5 Å for $MgSiO_3$ glass and 2.8 Å for Mg_2SiO_4 glass). Yellow sphere, magnesium; Red sphere, oxygen.

consistent with the coordination number derived from a combination of X-ray and neutron diffraction data (16, 17). However, the result of two recent NMR studies (14, 15) suggests that MgO_6 octahedra are the primary units in both $MgSiO_3$ glass and Mg_2SiO_4 glass (although 5-fold sites could not be ruled out). Attempts to include large fractions of MgO_6 polyhedra in our RMC simulations failed, even if the coordination number was calculated out to large distances i.e., 3.0 Å. Rather, in the case of Mg_2SiO_4 glass, the average Mg-O coordination number is found to be about 5 (corresponding a bond cutoff of 2.8 Å in the RMC model), which gives a very narrow ring size distribution as shown in Fig. 3*B*. In both glasses, a large fraction of 2-fold rings (edge-sharing) of MgO_x polyhedra are found, but $MgSiO_3$ glass yields a rather broad ring distribution of MgO_x.

In order to shed more light onto Mg-O coordination controversy, we performed DFT calculations for $MgSiO_3$ crystal and glass and for Mg_2SiO_4 crystal and glass. The results for the effective charges (Q_{eff}) and atomic volumes (V_{at}) of Mg are listed in

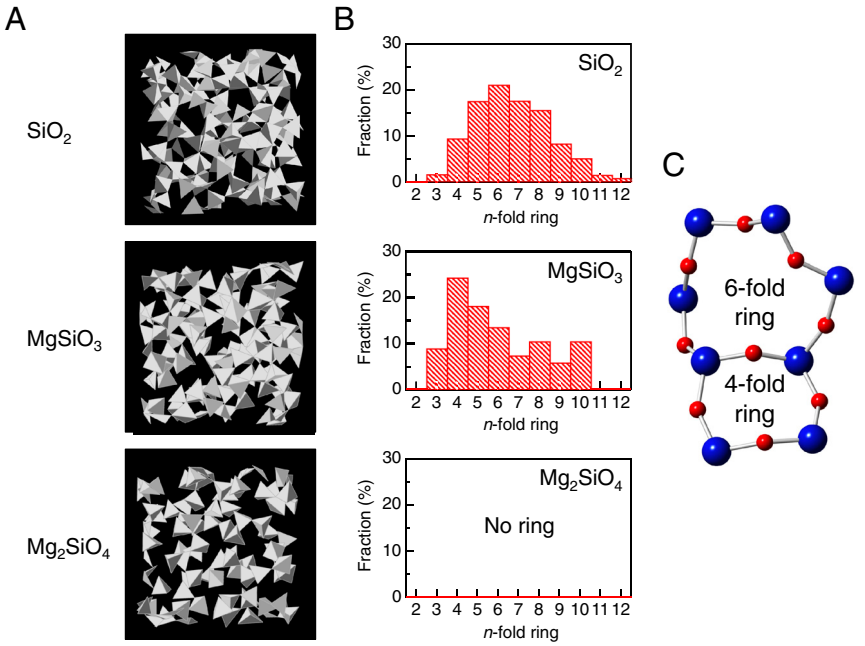

Fig. 2. The distribution of SiO_4 tetrahedra (*A*), ring statistics (*B*) of SiO_4 tetrahedra in SiO_2, $MgSiO_3$, and Mg_2SiO_4 glasses and a typical linkage of 4-fold and 6-fold Si-O rings (*C*). Red sphere, O; Blue sphere, Si.

Table 1. Atomic charges and volumes of Mg cations in $MgSiO_3$ and Mg_2SiO_4. Bader atom concept is based on electron density and its gradient (28)

System	Q_{eff} (Bader, *e*)	Q_{eff} (Voronoi, *e*)	V_{at} (Bader, Å^3)	V_{at} (Voronoi, Å^3)
$MgSiO_3$ glass (RMC)	-	-	-	13.36 (1.85)
$MgSiO_3$ glass (DFT)	+1.75 (0.01)	+1.25 (0.04)	5.96 (0.53)	12.69 (1.43)
$MgSiO_3$ crystal (DFT)	+1.76/+1.76	+1.25/+1.27	4.65/5.11	8.94/10.21
Mg_2SiO_4 glass (RMC)	-	-	-	11.83 (1.19)
Mg_2SiO_4 glass (DFT)	+1.73 (0.02)	+1.22 (0.04)	5.96 (0.56)	12.52 (1.42)
Mg_2SiO_4 crystal (DFT)	+1.74/+1.76	+1.19/+1.27	4.80/4.98	9.59/9.87

The values in parenthesis are standard deviations (errors). Atomic boundary is reached in a given direction once the gradient changes its sign and the electron density is integrated within the given volume in order to assign the atomic charge. Voronoi prescription of atomic volume is analogous to the Wigner-Seitz cell in crystalline materials. The crystalline structures comprise two classes of Mg, each, and values for both cases are displayed.

Table 1. The results show that Bader volumes are smaller than Voronoi volumes because the atomic boundary is closer to Mg than the geometric mean value (with oxygen). The resulting Q_{eff} values are correspondingly smaller for the Voronoi charges as there is more counterbalancing electron density inside the (larger) atomic volume of the cation. The effective charges (nominally +2) indicate a significant polarization effect between Mg and O, and some electron density has been transferred to Mg^{2+} which displays electrophilic nature.

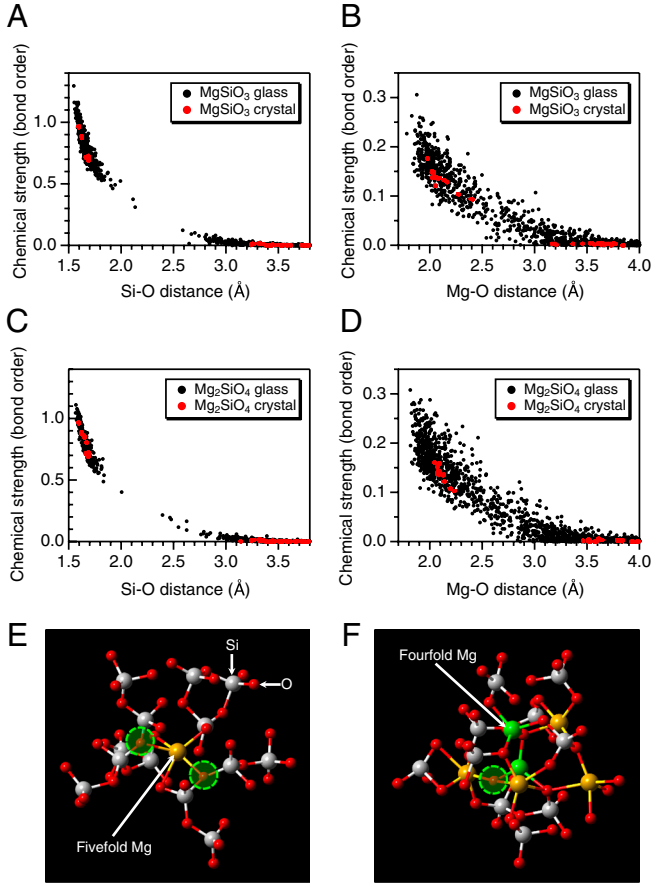

Fig. 4. Scatter plot of the chemical bond order as a function of distance for (*A*) Si-O pairs and (*B*) Mg-O pairs in the $MgSiO_3$ glass. The crystalline reference values are included in red, and the separation between bridging (longer) and terminal (shorter) Si-O bonds is visible. (*C and D*) The same for Mg_2SiO_4 glass where the crystalline phase comprises only terminal oxygens. (*E*) Snapshot of the local environment around an Mg cation in the $MgSiO_3$ glass. The 5-fold coordination of Mg is distorted and contacts with two bridging oxygens are highlighted. (*F*) Snapshot of the Mg_2SiO_4 glass where several Mg cations and their local environment is included. Both 4-fold and 5-fold coordination of Mg is visible, and a "free" oxygen, which does not participate in any silicate fragment but is shared by Mg, is highlighted.

The chemical bond orders for Si-O and Mg-O distances ("bonds") in $MgSiO_3$ and Mg_2SiO_4 are plotted in Fig. 4 *A–D*. The bond order concept is simple because a single covalent bond should produce a value close to unity and weaker types of chemical interaction appear as smaller values. The results for Si-O distances below 1.8 Å confirm this criterion and show that the values depend strongly on the bond length. For crystalline structures, we observe that the strong polarization interaction with Mg is reflected as a weakening of the terminal Si-O bonds in Mg_2SiO_4 (charge transfer from oxygen towards Mg), whereas the bridging Si-O bonds appear with smaller bond strenghts in $MgSiO_3$. There are also some defects in the silicate fragments in the glassy phase which appear as Si-O distances between 1.8–2.2 Å.

The Mg-O bond orders are smaller as the type of chemical interaction is different and they show an interesting scatter: While the data points for the crystalline (octahedral) bonds are within a small region, the Mg-O bonds appear in a broad range with a rapidly decreasing trend. The results indicate that a reasonable threshold for counting "bonds" lies around 2.5–2.6 Å, where the average value is of the same order as for some individual second-nearest-neighbor distances (maximum values for distances >3.0 Å). The DFT result for Mg-O coordination ranges between 4.4–5.0 and 4.5–5.2 Å for $MgSiO_3$ and Mg_2SiO_4, respectively, using bond cutoff distances of 2.5–2.8 Å. The corresponding DFT Mg-O pair distribution functions, $g_{ij}(r)$, show remarkably similar shapes for the first peak (nearest-neighbor distances) compared to that of the RMC structures (Fig. S4). The bond orders below 2.5 Å are generally larger than the corresponding crystalline values, and this is due to the fact that the Mg-O coordination is smaller in the glassy phase, where the cations compensate the smaller number of oxygen contacts by increasing the ionic bond strengths correspondingly. The compensation in bond strengths is also shown by the chemical coordination (valence) of Mg which has been counted by adding bond orders for each atom: The glassy phase results in values of 0.80 ± 0.02 ($MgSiO_3$) and 0.84 ± 0.02 ($MgSiO_4$), respectively, while the corresponding crystalline (octahedral) reference values are between 0.81–0.84.

The atomic charges and bond orders point out that the *effective* Mg-O interaction is very similar between the glassy and crystalline phase despite differences in geometrical coordination. The counter intuitive result found is that Mg in the glass occupies a *larger volume* with *less Mg-O contacts.* This feature is due to the irregular shapes of the coordination polyhedra, and is caused by the atomic disorder and misalignment of fragmented silica chains. Here, it is important to differentiate between the concepts of atomic volume [by Bader atom and Voronoi prescription (28)] and coordination polyhedron where the former can increase while the connections in the latter decrease. Selected snapshots of the Mg environment in $MgSiO_3$ and Mg_2SiO_4 glasses are displayed in Fig. 4 *E–F*, where we have highlighted Mg-coordinating bridging oxygens in the first case and a "free oxygen" in the latter case. The variation of O-Mg-O bond angles is evident in both, and

PHYSICS

Mg-O coordination ranges between 4 and 5. It is known that RMC produces the most disordered structure (35) which is consistent with a given set of diffraction data and geometrical constraints, and that DFT simulations may not achieve sufficient relaxation in the glass structure due to the long time scale. Experimentally the effect of quench rate can have an important effect on glass structure (36). The higher the cooling rate, the higher the fictive temperature and the resulting glass may correspond to a more disordered structure than the same system cooled at a slower rate. However, in this study we did not use any time scale-related calculations, so the resulting static model structure can be considered a snapshot consistent with the diffraction data. Nonetheless, the combination of methods used here provides a way of introducing energy and electronic structure into the RMC protocol (37). We note that in a similar DFT study by de Koker et al. (38) an Mg-O coordination number of 5.1 was reported for Mg_2SiO_4 melt at 3,000 K and ambient pressure.

In $MgSiO_3$, Mg binds to silicates (types Q_1, Q_2, and Q_3) via terminal *and* bridging oxygens similarly to the crystalline phase (Fig. S2). The free oxygens are absent in the crystalline Mg_2SiO_4, but they bind to Mg together with terminal oxygens (from Q_0 and Q_1 species) in the glassy phase. Typically, there are 3 to 4 Mg contacts for a free oxygen. Differences in the chemical environment of oxygen are reflected in its valence (summed bond orders), which reduces from 1.9 (bridging) to 1.6 (terminal), and to 1.1 (free oxygen). The valence of silicon is around 3.4–3.5 for all systems, and it should be compared with that of the formal covalent valence of 4.

The distribution of "-Si(Mg)-O-Si(Mg)-O-Si(Mg)-" rings in $MgSiO_3$ and Mg_2SiO_4 glasses are shown in Fig. 5 together with that of "-Si-O-Si-O-Si-" rings in SiO_2 glass. It is well known that glass forming ability (GFA) of Mg_2SiO_4 glass is lower than that of $MgSiO_3$ glass (7). As can be seen in Fig. 5, SiO_2 glass which has a high GFA, has a very broad ring distribution and is topologically disordered, whereas Mg_2SiO_4 glass which has a low GFA and a very narrow ring distribution is more topologically ordered. To further understand the glass structure and nature of the atomic packing, the atomic configurations together with the cavity volume are shown in Fig. 6. It is noted that SiO_2 glass has a cavity volume of 31.9% using the definition given in ref. 33, whereas both $MgSiO_3$ and Mg_2SiO_4 glasses have almost no cavities. The openness of the SiO_2 glass structure is maintained to retain the local order, and the disorder introduced by the addition of Mg-O results in a more compact structure due to the formation of MgO_5 and MgO_6 polyhedra. This trend is similar to $3Na_2O$-$4SiO_2$ and $3Na_2O$-$4SiO_2$ glasses (39) but is in sharp contrast to PbO-SiO_2 glass, in which more than 10% cavity volume is observed over a wide compositional range (33), which is a signature of high-glass forming ability. To understand the glass structure in detail, the connectivity of SiO_4 tetrahedra and MgO_x polyhedra were calculated and are compared to $3Na_2O$-$4SiO_2$ and 3CaO-$4SiO_2$ glasses in Table 2. The most striking feature is that the connectivity of SiO_4 tetrahedra and MgO_x polyhedra are almost the same for the $MgSiO_3$ and Mg_2SiO_4 RMC glass models. Furthermore, it is noted that MgO_x polyhedra tend to corner-share oxygens with SiO_4 tetrahedra, and a large amount of edge-shared MgO_x polyhedra are found in both $MgSiO_3$ and Mg_2SiO_4 glasses. Thus, the characteristic connectivity of MgO_x in $MgSiO_3$ and Mg_2SiO_4 glasses is the primary reason for "topologically ordered void free glasses" in this system.

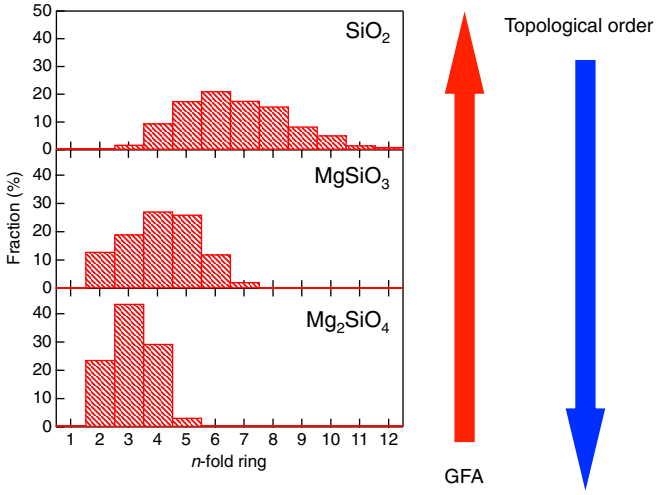

Fig. 5. The distribution of "-Si(Mg)-O-Si(Mg)-O-Si(Mg)-" rings in $MgSiO_3$ and Mg_2SiO_4 glasses and the distribution of "-Si-O-Si-O-Si-" rings in SiO_2 glass.

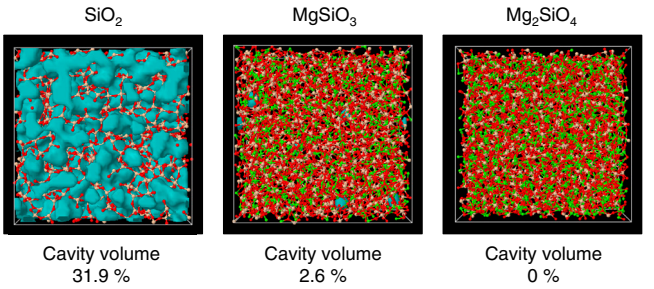

Fig. 6. The atomic RMC configuration and cavities of SiO_2, $MgSiO_3$ and Mg_2SiO_4 glasses. Light gray, silicon; Red, oxygen; Green: magnesium; Cyan isosurfaces: cavities (voids).

In this paper, we have focused on the structure of the glassy state due to the availability of neutron, X-ray, and NMR data. However, we have also performed RMC modeling on X-ray data from $MgSiO_3$ and Mg_2SiO_4 liquids (40), and combined the results with DFT molecular dynamics (MD) simulations. The X-ray total structure factors $S(Q)$ together with the experimental data (40) and the partial-pair distribution functions, $g_{ij}(r)$ of $MgSiO_3$ liquid (2,153 K) and Mg_2SiO_4 liquid (2,223 K) obtained from the final DFT-MD simulation are shown in Figs. S5 and S6, respectively. As can be seen in Fig. S5, agreement between X-ray data and the DFT-MD model is good (even without any refinement). The partials $g_{ij}(r)$ of Mg_2SiO_4 liquids are similar to those of $MgSiO_3$ liquid except for the Si-Si $g_{ij}(r)$ due the network deformation of SiO_4 tetrahedra in the former. The results on the liquids give similar Mg-O coordination numbers [$N_{Mg\text{-}O} = 4.03$ in $MgSiO_3$ liquid (up to 2.5 Å) and 4.79 (up to 2.8 Å) while $N_{Mg\text{-}O} = 4.19$ in Mg_2SiO_4 liquid (up to 2.5 Å) and 5.02 (up to 2.8 Å)] and connectivities to those presented here for the glasses.

The DFT calculations explain the discrepancy between the NMR and diffraction results, because NMR probes chemical shifts which are very sensitive to the electronic environment of the nuclei, while diffraction is a direct probe of the *average* coordination number through known neutron scattering lengths or the number of electrons surrounding an atom (provided the partial functions are known). Previous studies (14, 15) concluded that for $MgSiO_3$ and Mg_2SiO_4 glasses, the NMR shifts are in line with the octahedral crystalline environment, although in this

Table 2. The connectivity analysis of SiO_4 and MO_x (M = Mg, Na, Ca) units in silicate glasses

	$MgSiO_3$	Mg_2SiO_4	$3Na_2O$-$4SiO_2$ (39)	3CaO-$4SiO_2$ (39)
SiO_4-SiO_4	corner 100%	corner 100%	corner 100%	corner 100%
SiO_4-MO_x	corner 86.9%	corner 87.1%	corner 75.3%	corner 72.7%
	edge 13.1%	edge 12.9%	edge 22.8%	edge 24.3%
	face 0%	face 0%	face 1.9%	face 3.0%
MO_x-MO_x	corner 75.3%	corner 76.1%	corner 78.8%	corner 78.1%
	edge 23.7%	edge 23.4%	edge 19.6%	edge 20.4%
	face 1.0%	face 0.5%	face 1.6%	face 1.5%

study we find that the Mg-O coordination is actually smaller in the glasses. This result is counter intuitive because the Mg atoms occupy larger atomic volumes in the glassy state and the MgO_x polyhedra have become irregular. The underlying reason for the behavior is due to the compensation of Mg-O bond strengths (polarization) and weak dependence on the directionality. Presumably, application of higher pressure, as in Earth's mantle, would bring the MgO_x polyhedra closer to the regular octahedral shape, but this would require structural adjustments in the silica units as evidenced by X-ray Raman scattering measurement for $MgSiO_3$ glass (8). DFT computations of Mg_2SiO_4 melts under pressure have shown that the Mg-O coordination becomes 6-fold at 10–20 GPa and increases towards 8 at higher pressures (38). The structural glass model presented here at ambient pressures does however explain the low viscosity of highly mobile ultramafic lavas. The lack of polymerized silicate units and range of distorted Mg environments in the liquid state are consistent with quiescent lava flows that are more strongly affected by gravitational forces. These model glass structures are substantially different from the corresponding crystalline phases and demonstrated the powerful combination of diffraction and DFT simulation in unraveling their complicated structures. Furthermore, the atomic models describe an amorphous Mg-based network which could lead to the formation of new families of lightweight glasses, glass ceramics or cements with no porosity.

ACKNOWLEDGMENTS. We thank Dr. Jan Swenson for providing us with the atomic configuration of $3Na_2O$-$4SiO_2$ and $3CaO$-$4SiO_2$ glasses. We thank Mr. Hiroyuki Fujii for helping the development of software for ring statistics calculations. The synchrotron radiation experiment was carried out with the approval of the Japan Synchrotron Radiation Research Institute (JASRI) (Proposal No. 2006B1461) and all DFT calculations were carried out on Juropa (Xeon 5570) and Cray XT4/XT5 supercomputers in the Forschungszentrum Jülich (FZJ, Germany) and CSC (Espoo, Finland) with grants from FZJ, the John von Neumann Institute for Computing, and CSC. This work was supported by the Department of Energy, Division of Materials Science, Office of Basic Energy Science, under Contract number DE-AC02-06CH11357 and by Grant-in-Aid for Scientific Research on Innovative Areas (Grant No. 20103004) from the Ministry of Education, Culture, Sports, Science, and Technology of Japan. S.K. and J.A. are supported by the Japan Science and Technology Agency and the Academy of Finland via the Strategic Japanese-Finland Cooperative Program on "Functional Materials."

1. Zachariasen WH (1932) The atomic arrangement in glass. *J Am Chem Soc* 54:3841–3851.
2. Cooper AR (1978) Zachariasen's rules, Madelung constant, and network topology. *Phys Chem Glasses* 19:60–68.
3. Gupta PK, Cooper AR (1990) Topologically disordered networks of rigid polytopes. *J Non-Cryst Solids* 123:14–21.
4. Rino JP, Ebbsjö I, Kalia RK, Nakano A, Vashishta P (1993) Structure of rings in vitreous SiO_2. *Phys Rev B* 47:3053–3062.
5. Kohara S, Suzuya K (2004) Intermediate-range order in vitreous SiO_2 and GeO_2. *J Phys: Condens Mat* 17:S77–S86.
6. Weber JKR, Felten JJ, Cho B, Nordine PC (1998) Glass fibres of pure and erbium- or neodymium-doped yttria-alumina compositions. *Nature* 393:769–771.
7. Tangeman JA, et al. (2001) Vitreous forsterite (Mg_2SiO_4): Synthesis, structure, and thermochemistry. *Geophys Res Lett* 28:2517–2520.
8. Shim S-H, Catalli K (2009) Compositional dependence of structural transition pressures in amorphous phases with mantle-related compositions. *Earth and Planet Sci Lett* 283:174–180.
9. Lee SK, et al. (2008) X-ray Raman scattering study of $MgSiO_3$ glass at high pressure: implication for triclustered $MgSiO_3$ melt in earth's mantle. *Proc Nat Acad Sci USA* 105:7925–7929.
10. Stebbins JF, Farnan I (1992) Effects of high temperature on silicate liquid structure: a multinuclear NMR study. *Science* 255:586–589.
11. Williams Q, McMillan P, Cooney TF (1989) Vibrational spectra of olivine composition glasses: the Mg-Mn join. *Phys Chem Miner* 16:352–359.
12. Durben DJ, McMillan PF, Wolf GH (1993) Raman study of the high-pressure behavior of forsterite (Mg_2SiO_4) crystal and glass. *Am Mineral* 78:1143–1148.
13. Sen S, Tangeman JA (2008) Evidence for anomalously large degree of polymerization in Mg_2SiO_4 glass and melt. *Am Mineral* 93:946–949.
14. Shimoda K, Tobu Y, Hatakeyama M, Nemoto T, Saito K (2007) Structural investigation of Mg local environments in silicate glasses by ultra-high field ^{25}Mg 3QMAS NMR spectroscopy. *Am Mineral* 92:695–698.
15. Sen S, Maekawa H, Papatheodorou GN (2009) Short-range structure of invert glasses along the pseudo-binary join $MgSiO_3$-Mg_2SiO_4: results from ^{25}Si and ^{25}Mg MAS NMR Spectroscopy. *J Phys Chem B* 113:15243–15248.
16. Wilding MC, Benmore CJ, Tangeman JA, Sampath S (2004) Coordination changes in magnesium silicate glasses. *Europhys Lett* 67:212–218.
17. Kohara S, et al. (2004) Glass formation at the limit of insufficient network formers. *Science* 303:1649–1652.
18. Wilding MC, Benmore CJ, Tangeman JA, Sampath S (2004) Evidence of different structures in magnesium silicate liquids: coordination changes in forsterite- to enstatite-composition glasses. *Chem Geol* 213:281–291.
19. Cormier L, Cuello GJ (2011) Mg coordination in a $MgSiO_3$ glass using neutron diffraction coupled with isotopic substitution. *Phys Rev B* 83:224204–224208.
20. McGreevy RA, Pusztai L (1988) Reverse Monte Carlo simulation: a new technique for the determination of disordered structures. *Mol Simulat* 1:359–367.
21. CP2K Developers Group, (2000–2011), http://cp2k.berlios.de.
22. VandeVondele J, et al. (2005) QUICKSTEP: Fast and accurate density functional calculations using a mixed Gaussian and plane waves approach. *Computer Physics Communications* 167:103–128.
23. Goedecker S, Teter M, Hutter J (1996) Separable dual-space Gaussian pseudopotentials. *Phys Rev B* 54:1703–1710.
24. VandeVondele J, Hutter J (2007) Gaussian basis sets for accurate calculations on molecular systems in gas and condensed phases. *J Chem Phys* 127:114105–114109.
25. Perdew JP, Burke K, Ernzerhof M (1996) Generalized gradient approximation made simple. *Phys Rev Lett* 77:3865–3868.
26. Carlson WD, Swinnea JS, Miser DE (1988) Stability of orthoenstatite at high temperature and low pressure. *Am Mineral* 73:1255–1263.
27. Hazen RM (1976) Effects of temperature and pressure on the crystal structure of forsterite. *Am Mineral* 61:1280–1293.
28. Tang W, Sanville E, Henkelman G (2009) A grid-based Bader analysis algorithm without lattice bias. *J Phys: Condens Mat* 21:084204–084207.
29. Guttman L (1990) Ring structure of the crystalline and amorphous forms of silicon dioxide. *J Non-Cryst Solids* 116:145–147.
30. Le Roux S, Jund P (2010) Ring statistics analysis of topological networks: new approach and application to amorphous GeS_2 and SiO_2 systems. *Comp Mater Sci* 49:70–83.
31. Akola J, Jones RO (2007) Structural phase transitions on the nanoscale: the crucial pattern in the phase-change materials $Ge_2Sb_2Te_5$ and GeTe. *Phys Rev B* 76:235201–235210.
32. Salmon PS, Martin RA, Mason PE, Cuello GJ (2005) Topological versus chemical ordering in network glasses at intermediate and extended length scales. *Nature* 435:75–78.
33. Kohara S, et al. (2010) Lead silicate glasses: binary network-former glasses with large amounts of free volume. *Phys Rev B* 82:134209-1–134209-7.
34. Shannon RD (1976) Revised effective ionic radii and systematic studies of interatomic distances in halides and chalcogenides. *Acta Crystallogr* 32:751–757.
35. Dove MT, Tucker MG, Keen DA (2002) Neutron total scattering method: simultaneous determination of long-range and short-range order in disordered materials. *Eur J Mineral* 14:331–348.
36. Sato RK, McMillan PF, Dennison P, Dupree R (1991) High-resolution aluminum-27 and silicon-29 MAS NMR investigation of silica-alumina glasses. *J Phys Chem* 95:4483–4489.
37. Akola J, et al. (2009) Experimentally constrained density-functional calculations of the amorphous structure of the prototypical phase-change material $Ge_2Sb_2Te_5$. *Phys Rev B* 80(R):020201-1–020201-4.
38. de Koker NP, Stixrude L, Karki BB (2009) Thermodynamics, structure, dynamics, and freezing of Mg_2SiO_4 liquid at high pressure. *Geochim Cosmochim Ac* 72:1427–1441.
39. Karlsson C, et al. (2005) Structure of mixed alkali/alkaline-earth silicate glasses from neutron diffraction and vibrational spectroscopy. *Phys Rev B* 72:064206–064212.
40. Wilding MC, Benmore CJ, Weber JKR (2010) Changes in the local environment surrounding magnesium ions in fragile MgO-SiO_2 liquids. *Europhys Lett* 89:26005-1–26005-5.